JOURNAL OF MATERIALS SCIENCE **33** (1998) 5037–5047

The measurement of compressive creep deformation and damage mechanisms in a single-phase alumina

Part I *Grain boundary sliding*

C. R. BLANCHARD, R. A. PAGE
Southwest Research Institute, San Antonio, TX 78228, USA
E-mail: cblanchard@swri.org

Grain boundary sliding (GBS) has been hypothesized to act as the primary driving force for the nucleation and growth of grain boundary cavities in ceramics undergoing creep. In addition, GBS is often a major mode of deformation during high-temperature creep. This paper demonstrates the importance of GBS with mode II GBS measurements performed using a stereoimaging technique on a single-phase alumina tested under constant compressive stresses of 70 and 140 MPa at 1600 °C. Measurements were taken at constant time intervals during creep. The results support previous observations that GBS is stochastic and history independent. GBS displacements at given time intervals are shown to fit a Wiebull distribution. During steady-state creep, GBS displacements increased linearly with time at a constant sliding rate of $\approx 6.0 \times 10^{-5}$ μm s^{-1} at 70 MPa and $\approx 1.3 \times 10^{-4}$ μm s^{-1} at 140 MPa. Also, an average of 67% of the grain boundaries exhibited measurable sliding throughout the creep life of the 140 MPa test. Results of the GBS measurements are used to modify an existing creep model describing stochastic GBS. In part II of this paper [1], the GBS measurements reported are related to the associated creep cavitation measured in specimens tested under identical conditions.

1. Introduction

The time-dependent deformation of a polycrystalline ceramic at elevated temperatures can only be achieved by the relative movement of adjacent grains (grain boundary sliding); a shape change of individual grains through slip, twinning or diffusion; or porosity changes. These deformation processes are often synergistic and lead to creep damage and failure. The specific mechanisms governing creep deformation, damage, and failure will, of course, depend on the material type and microstructure [2, 3].

In structural ceramics, failure caused by creep is often caused by the stress-induced nucleation, growth, and coalescence of cavities on grain boundaries, which eventually leads to crack formation and failure [4–8]. Grain boundary sliding (GBS) has been hypothesized to be the primary driving force for creep cavitation, whereby the relative grain displacements give rise to stress concentrations at critical locations on the grain boundaries, such as second-phase particles, triple points, and ledges, where GBS and associated creep cavities have been observed [9–14]. GBS is also known to be an important mechanism in superplastic deformation, as has been noted in polycrystalline alumina [15] and in a Zirconia-Alumina composite [16].

Although GBS has been discussed and proposed as an important deformation and damage process during creep of ceramic materials, no comprehensive study of GBS during creep has yielded details of the GBS phenomenon itself. Reports in the literature of GBS measurements in ceramics are limited [15–31]. Some measurements have been performed on bicrystal systems [30, 31] which are not considered to be representative of the three-dimensional constraint imposed by the surrounding grains of a polycrystalline material. Most of the studies [21–24, 26, 27] focused on indirect measurement techniques, such as the so-called grain-shape-change technique (which has been shown not to be accurate [32]) that only yielded the GBS contribution to the total creep strain. One study only provided GBS data in the form of a qualitative comparison of microstructural features post-test [22]. Chokshi [15] and Nixon and Davies [28] have published GBS measurements on Al_2O_3 and SiC, respectively, using the line offset method. Although their data illustrated the importance of GBS to the creep process, the results were only reported in terms of the GBS contribution to creep deformation. In addition, Blanchard and Page have published studies [17–19] reporting GBS microdisplacement, strain, and strain rate measurements resulting from compressive creep of Al_2O_3 and showed that measurable sliding occurs as mode II shear, in-plane rotation, and in-grain shear. Although these studies showed the importance of GBS to creep deformation, the extent

of GBS, and the various types of sliding in ceramics, no GBS measurements to date have been documented during the creep process to show details of the sliding microdisplacements and kinetics.

Calculations performed by Raj [33] and Argon [34] have shown that stresses on the order of five to 20 times the remote applied stress are needed in order to nucleate stable creep cavities. Argon [35] has hypothesized that GBS can give rise to the stress concentrations needed for cavitation. Furthermore, Chan *et al.* [11] have shown that for a ledge acting as a stress concentration on a sliding grain boundary, the localized tensile stress is of sufficient magnitude for stable cavities to nucleate during only a short time period as a result of the competition of diffusional stress relaxation. Blanchard and Page [18] calculated strains resulting from GBS displacements measured on individual Al_2O_3 grain boundaries of 4000% (corresponding to a strain rate of 2×10^{-2} s^{-1}), thereby providing experimental evidence that large localized stress concentrations caused by GBS are possible. Through mathematical models, GBS has been shown to relate to both continuous cavity nucleation [36] and transient cavity growth [37]. In Chan and Page's model [36, 37], cavitation was shown to depend on the number and magnitude of GBS events and the rate of GBS. It is this critical GBS data that currently lacks in the literature, particularly in materials for which cavitation kinetics are well characterized.

There are a number of complications associated with performing GBS measurements. The simplest experiments use bicrystals which allow facile measurement and interpretation of the data. Unfortunately, as previously mentioned, bicrystal data does not represent the constraint provided by the surrounding grains in polycrystalline materials. In addition, the three-dimensional grain structure found in polycrystalline materials presents experimental complications for performing meaningful GBS measurements. These complications arise mainly as a result of the three-dimensional network of grains sliding in innumerable combinations, magnitudes and directions and the difficulties in marking the grains and measuring the sliding displacements, especially at the interior of the specimen. For a number of reasons, performing these measurements on ceramic materials (as opposed to metals) further complicates a GBS experiment. Historically, it has been difficult to mark effectively a ceramic microstructure to provide the reference needed to observe the relative grain motion resulting from GBS. In addition, the high test temperatures employed to creep ceramics often change or destroy these surface markings.

In this paper, GBS measurements, including displacements over time, GBS rates, and GBS frequency, taken during creep of Al_2O_3 will be reported. Measurements were made using an automated machine-vision-based stereoimaging system assembled to record microdisplacements and strain in the microstructures of materials. The vision system is an automated version of the stereoimaging technique. Stereoimaging compares two photographs that show in-plane displacements in one relative to the other. In a stereoscope, these displacements are perceived in the third dimension and may be measured using photogrammetric methods [38].

The stereoimaging technique has proven to be very powerful in that areas of a microstructure may be analysed and periodic GBS displacement arrays may be generated along the entire length of grain boundaries. In addition, the technique does not require the use of linear markers, such as scratches or fiducial grids which can only provide for a GBS measurement at one point on a given grain boundary. This automated stereoimaging technique has also been used to successfully measure various aspects of crack nucleation and growth in metals and composites [39–42].

This paper will report on the results of a comprehensive study of the GBS behaviour of a single-phase Al_2O_3 undergoing creep at two stress levels. The GBS histories of individual grains will show that GBS is in fact stochastic and history independent. Periodic GBS measurements taken over time will show that sliding displacements, on average, increase linearly with time and strain during steady state creep. The relationship between the GBS rate and applied stress will be discussed. These results are also used to modify an existing creep model describing stochastic GBS. Part II of this paper will correlate these GBS measurements with creep cavitation measurements made on the same material under identical conditions. Microstructural evidence of GBS and creep cavitation documented from these experiments has been published previously [13].

2. Experimental procedure

2.1. Material

Lucalox® Al_2O_3, with an average grain size of 17 μm, was selected for this study because of its relatively large equiaxed grains and glass-free grain boundaries, characteristics which together provided for fewer complications when digitizing the microstructures. Lucalox® is composed of 99.9% pure Al_2O_3 doped with MgO as a sintering aid. Although $MgAl_2O_4$ spinel particles have been identified at triple points [43, 44], the microstructure of Lucalox® is relatively clean and free from any glassy phase or regular second-phase precipitates.

2.2. Specimen preparation

Compressive creep specimens were machined into right circular cylinders, 1.27 cm in length and 0.64 cm in diameter. The specimen ends were ground and lapped flat and parallel to within 5 μm.

To maintain a continuous record of the microstructural state during the creep life of the specimen, polymer replicas were taken after each test interval. These replicas were subsequently used to perform the GBS measurements. For this purpose, a polished flat, 1.27 cm in length and 0.25 cm in width, was ground and lapped on the front radial surface of the cylindrical specimens. The specimens were thermally etched for 1 hr at 1600 °C in air to delineate the grain boundaries, and replicas were taken to characterize the precrept, baseline microstructure. The surface features needed to make the appropriate GBS measurements using the machine vision system were formed when molybdenum

plated onto the polished and etched specimen surface from the molybdenum heat shield during creep testing.

2.3. Creep tests

Compressive creep tests were performed on the as-sintered, machined, and etched specimens in a titanium-gettered argon atmosphere at 1600 °C using a dead-weight-loaded machine. Specimens were tested for GBS measurements under stress levels of 140 MPa and 70 MPa.

The creep tests were interrupted periodically (every 30 min for the 140 MPa tests and 60 or 120 min for the 70 MPa tests) to allow the polymer replicas to be taken, during which time a stress of 20 MPa was maintained. For each replicating interval, the specimens were cooled under the test load to preserve the high temperature microstructure. The 140 MPa creep test was continued for 150 min (five replicating cycles), while the 70 MPa test ran for 540 min (seven replicating cycles) and was continued for another 480 min, replicated, crept again for 60 min, and replicated.

To record the microstructural creep history for subsequent microdisplacement measurements, replicas of the polished and etched flat surfaces of the creep specimens were taken after each 30, 60 or 120 min test interval over the duration of the entire test. The replicas were then flattened and mounted on glass slides, coated with aluminum to enhance contrast, and photographed. Specifically, several series of pictures were taken at a magnification of 500× at various locations on the replicas, providing a visual history of the microstructural evolution (of groups of 15–20 grains) during creep. These series of photographs were then analysed, using the machine-vision system, to obtain the relative grain displacements and strains in the microstructure resulting from the creep test.

2.4. GBS measurements

GBS measurements were made by digitizing micrograph pairs representing a creep test interval on a specialized DISMAP system. The DISMAP system (measurement of micro-*dis*placements by *ma*chine vision *p*hotogrammetry), developed by Franke *et al.* [45] includes a Cognex 2000 image processing system, which provides fast correlated searching for pattern matching combined with standard image processing capabilities. A detailed description of the hardware and operation of the machine vision system is provided elsewhere [45].

In general, photograph pairs representing the microstructural evolution during a creep interval (for example a 30-min creep interval from 120 to 150 min from the 140 MPa test) were placed under the two stereo cameras, aligned, digitized, and saved for further processing. The GBS displacement measurements were made by assigning points at which measurements were to be made by superimposing a digitized grid over the grain pairs and executing a programmed search and train sequence. For consistency and referencing purposes, grain boundaries were aligned parallel to the y-axis of the grid and placed at $x = 0$ to define the grain boundary location for subsequent analysis. The results for each grain boundary of the DISMAP measurements were displacement arrays superimposed over each grain pair, showing the relative grain movement and deformation during the given time interval. Data gathered on and near the grain boundaries were ignored to remove any erroneous results due to grain boundary grooving from thermal etching. GBS data were gathered on a total of 70 grain boundaries (from 10 randomly-chosen areas in the microstructure) over four time intervals for the 140 MPa test (starting after 30 min of testing because of lack of required surface features in the baseline microstructure) and eight grain boundaries over eight time intervals for the 70 MPa test (starting after 180 min of testing because of lack of required surface features in the baseline microstructure). The grain boundaries were chosen for measurement at random to provide data representing the average behaviour of the specimen.

3. GBS results

3.1. Creep characteristics

Because a dead-weight-loaded creep rig with no extensometry was used for the compressive creep tests, no displacement versus time curves were recorded. Instead, at the end of each test interval, the specimens were removed from the load train and dimensioned, and the strain accumulated over the given time interval was calculated.

The linear relationships between strain and time observed for both the 140 MPa and 70 MPa tests show that, within the error of measurement, the specimens were in the steady-state creep regime during the time intervals used for GBS measurements. The specimen tested at 140 MPa failed after 151 min of creep and accumulated 0.63% strain at an average rate of 7×10^{-7} s^{-1}. The 70 MPa specimen was tested for a total of 1080 min and accumulated 0.72% strain at an average rate of 1×10^{-7} s^{-1}.

3.2. 140 MPa test results

Selected results of the mode II GBS measurements performed on individual grain boundaries are summarized in Fig. 1 where the mode II GBS displacement, $\overline{\mathrm{d}y}_{\mathrm{GB}}$, is plotted for each grain boundary in two microstructural areas examined versus the four, 30 min time intervals over which GBS measurements were made (for brevity, the remaining five microstructural areas are not presented in this detail). By examining the activity of the individual grain boundaries in each microstructural area, the GBS behaviour during creep may be characterized. For example, in microstructural area 1 (Fig. 1a) during the first time period in which measurements were made (30–60 min), the ten grain boundaries measured exhibited a distribution (to be described later) of mode II GBS displacements ranging from 0.06 μm to 0.59 μm, while three grain boundaries exhibited no measurable sliding. During the next time interval (60–90 min), a given individual grain boundary was observed to either slide (either more or less than in the first time period) or not slide. More specifically,

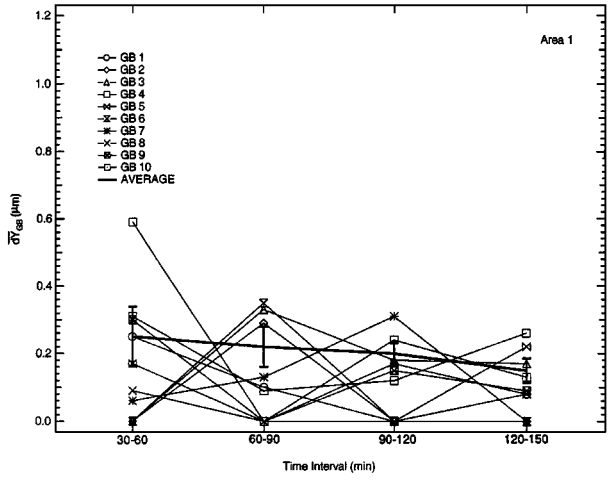

(a)

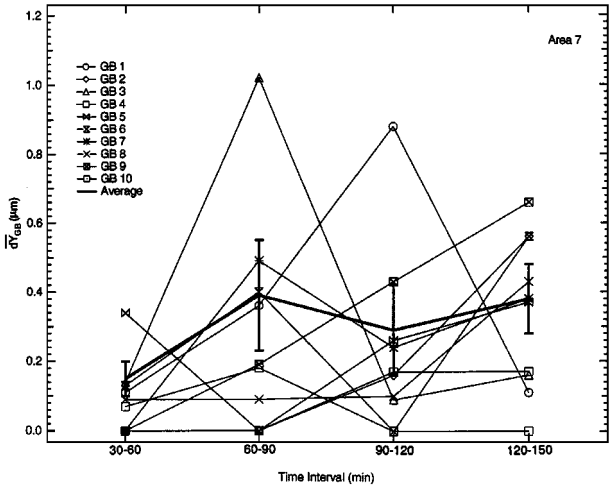

(b)

Figure 1 Mode II GBS displacements measured during the 140 MPa compressive creep test versus creep time interval of individual grain boundaries in (a) Area 1, and (b) Area 7.

a given grain boundary can either not slide, or exhibit either a larger or smaller GBS displacement in successive creep time intervals. In other words, the GBS events are stochastic in nature. This behaviour is also observed in microstructural area 7 (Fig. 1b) where some larger $\overline{dy}_{GB}$ values were measured and was also observed throughout all of the time intervals in each of the remaining five microstructural areas not shown. These results indicate that the Lucalox® exhibits random GBS behaviour over time during compressive creep.

The average GBS displacement of only those boundaries that slid is represented as the bold line with standard deviation bars in Fig. 1 (a and b). The average GBS displacements (of only those boundaries that slid) for each of the seven microstructural areas are combined in Fig. 2. Note that in areas 1–4 and 6, the average of the sliding displacements remains constant over creep time within the error of one standard deviation. In contrast, the average sliding displacement in areas 5 and 7 appears to increase slightly with creep time. Also, the average GBS displacement over time behaves differently in each area measured. These data further support the

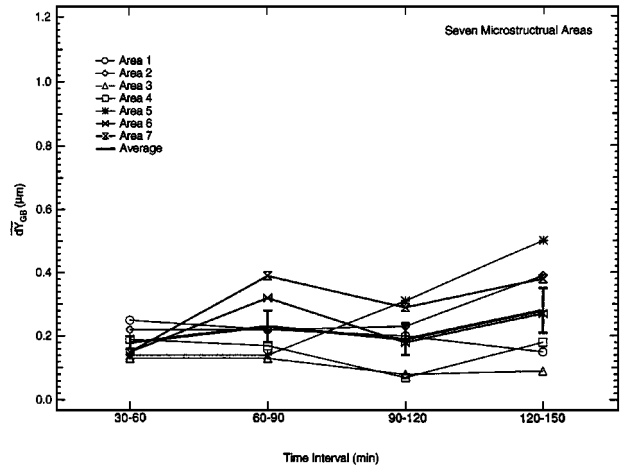

Figure 2 Average mode II GBS displacements (only of those boundaries that slid) of each microstructural area. The bold line shows the average mode II GBS displacements of all boundaries measured.

previous observation that the GBS behaviour is stochastic, even when averaged within a given microstructural area. In addition, the results of the GBS measurements in areas 5 and 7 suggest that some groups of grains in a sample will exhibit increased GBS activity with time, possibly leading to a site where creep cavitation behaviour is accelerated, or where microcracks will form.

When the mode II GBS measurements for all 70 grain boundaries are averaged together (indicated by the bold line with standard deviation bars in Fig. 2), there appears to be a slight increase during the last time interval (120–150 min) in the magnitude of the overall average GBS displacement measured. This small increase, however, is not considered to be statistically significant, as the increase observed is just above the standard deviation bars of the data gathered during the previous three time intervals. In addition, the increase in $\overline{dy}_{GB}$ for all the grain boundaries during the 120–150 min time interval is primarily caused by the large displacements measured in areas 5 and 7. Thus, although the average mode II GBS displacement measured did not increase significantly with creep time, small areas (containing $\approx$ 15–20 grains) in the microstructure were observed to exhibit an increase in the average GBS displacement with creep time.

The results of a survey recording the GBS history of each grain boundary in the seven microstructural areas over the four creep time intervals (30–60, 60–90, 90–120, and 120–150 min) are shown in Fig. 3. The four GBS displacement measurements ($\overline{dy}_{GB}$ values measured over the four time intervals) for each grain boundary were classified in a binary manner by labelling zero measurable displacement, N (no movement), and any measurable displacement, M (movement), regardless of the magnitude of the displacement. As seen in Fig. 3, the four time periods give rise to 16 possible permutations of grain boundary activity. For example, 5.7% of the grain boundaries measured exhibited an N–M–N–N history during the four time intervals, thereby demonstrating four discrete intervals of movement. Specifically, these boundaries did not slide from 30 to 60 min, slid during the following 60 to 90 min period, and finally did not move from 90 to 120 min or from 120 to

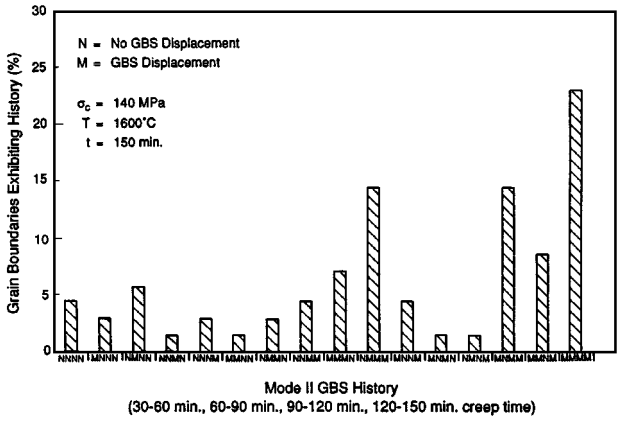

Figure 3 Mode II GBS history over four time intervals during creep, where N represents no GBS and M represents sliding during the given 30 min interval.

150 min. The results in Fig. 3 again support the previous observation that Lucalox® exhibits stochastic GBS behaviour over creep time.

Also, through analysis of the data in Fig. 3, GBS does not appear to be history dependent. As no type of history permutation appears to exhibit a significant dominance over the average frequency of all the histories observed, the probability of a grain boundary moving in a given successive time period is the same as the frequency of boundaries moving at any given time in the bulk and is independent of previous grain boundary movement history. These results indicate that Lucalox® exhibits stochastic, history-independent GBS during compressive creep. The most frequent permutation observed was the M–M–M–M history (representing grain boundaries that moved during every time period), which was exhibited by $\approx 23\%$ of the grain boundaries measured and the next most frequent permutations observed where the N–M–M–M and the M–N–M–M, which were both exhibited by $\approx 14\%$ of the boundaries measured. The fact that the previously mentioned GBS histories were observed at higher frequencies than the average (7%) may be explained based on the average percentage of grain boundaries that slid (to be discussed in detail later). It will be shown that almost 70% of the grain boundaries measured exhibited GBS. Therefore, one would expect the permutations containing the most "movement" components to exhibit a higher frequency.

As previously mentioned, the individual GBS displacements measured during a given time interval represent some distribution of $\overline{dy}_{GB}$ values at each time interval. To determine which statistical model best represents the distribution of mode II GBS displacements, the data were subjected to a statistical analysis, specifically, a comparison test described by Wirsching and Carlson [46], which included five of the more commonly used probability density functions (PDF): normal, lognormal, exponential, Weibull, and extreme value distribution (EVD). The comparison study was performed by calculating two statistics, the Cramer–Von Mises (CVM) [46] and Finkelstein–Schafer (F–S) statistics [47] which are based on deviations between the hypothesized and empirical PDFs. The minimum CVM and F–S values for a given distribution represented the best fit.

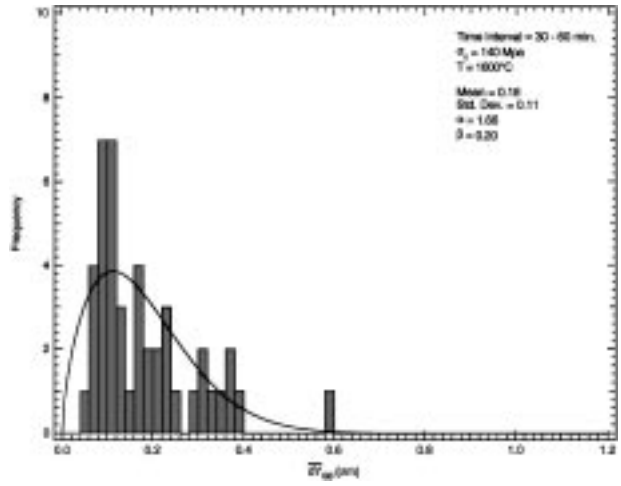

(a)

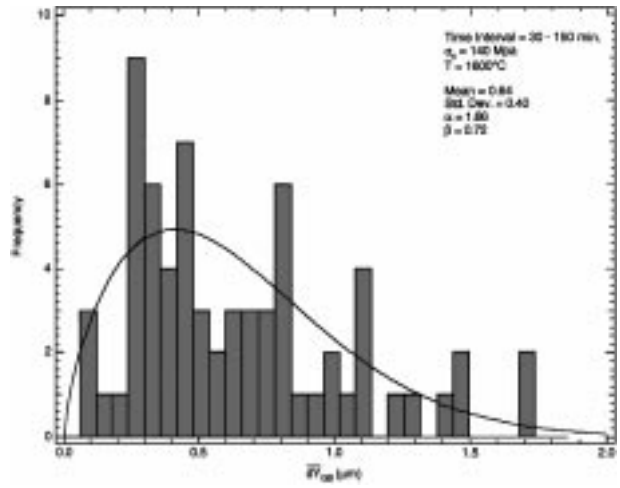

(b)

Figure 4 Frequency versus mode II GBS displacement (of only those boundaries that slid) and Weibull distribution for (a) 30–60 min, and (b) cumulative (30–150 min) creep time intervals.

The statistical analysis revealed that the Weibull distribution [48] most appropriately represented the GBS displacement data. This is demonstrated in Fig. 4, which shows both the raw data histograms and the Weibull fit for the 30–60 min (Fig. 4a) and cumulative (over all four time intervals, 30–150 min) time intervals (Fig. 4b), respectively. The PDF for the Weibull distribution is defined as follows [48]

$$f(x) = \left(\frac{\alpha}{\beta}\right)\left(\frac{x}{\beta}\right)^{\alpha-1} \exp\left[-\left(\frac{x}{\beta}\right)^{\alpha}\right] \qquad (1)$$

where x represents the $\overline{dy}_{GB}$ values, α is the shape parameter, and β is the scaling parameter. Table I lists the Weibull parameters for each time interval and the cumulative data.

Comparing the Weibull parameters for each creep time interval reveals that, within experimental scatter, the distributions of mode II GBS displacements remain the same; neither the mean values nor the distributions shift significantly with creep time. In addition, the distribution of the cumulative mode II GBS displacements, determined by summing $\overline{dy}_{GB}$ values for each grain

TABLE I Mode II GBS displacement Weibull statistics (140 MPa compressive creep test)

Time Interval (min)	Mean $\overline{dy}_{GB}$ (μm)	Standard deviation (μm)	α	β
30–60	0.18	0.11	1.66	0.20
60–90	0.23	0.19	1.32	0.25
90–120	0.19	0.16	1.39	0.22
120–150	0.30	0.22	1.43	0.33
Average			1.45	0.25
Standard deviation			0.15	0.06
Cumulative (30–150)	0.64	0.40	1.66	0.72

boundary over all four time intervals, is consistent with the distributions for each individual time interval (also see Fig. 4b). This finding is significant because it indicates that the cumulative GBS behavior on a given grain boundary is the same as that observed at each time interval during steady-state creep (of course, the cumulative GBS displacement value will increase over time).

When the α and β values determined at each time interval are averaged, the mode II GBS displacements over a 30-min time interval in Lucalox® crept at 140 MPa at 1600 °C can be defined as follows

$$f(\overline{dy}_{GB})_{30\ min} = 6\left(\frac{\overline{dy}_{GB}}{0.25}\right)^{0.5} \exp\left[-\left(\frac{\overline{dy}_{GB}}{0.25}\right)^{1.5}\right] \quad (2)$$

Similarly, the cumulative mode II GBS displacements measured over all four 30-min time intervals under the same creep conditions may be defined as

$$f(\overline{dy}_{GB})_{cum} = 2\left(\frac{\overline{dy}_{GB}}{0.72}\right)^{0.5} \exp\left[-\left(\frac{\overline{dy}_{GB}}{0.72}\right)^{1.5}\right] \quad (3)$$

using a value of 1.5 for α (obtained by averaging the cumulative and interval α values) and $\beta = 0.72$. These empirically derived descriptions of the interval and cumulative GBS displacements will later be applied to a model developed by Chan and Page [36] to describe stochastic GBS behavior.

Since the average $\overline{dy}_{GB}$ measured over the seven, randomly chosen microstructural areas remains constant during the creep life of the 140 MPa specimen, the cumulative average $\overline{dy}_{GB}$ increases linearly with time, as shown in Fig. 5. The cumulative average $\overline{dy}_{GB}$ was calculated by adding the average $\overline{dy}_{GB}$ values over successive time intervals. This represents the accumulated damage resulting from GBS over creep time. Thus, during steady-state compressive creep under a load of 140 MPa, the cumulative GBS displacements increase linearly with creep time. Using the data presented in Fig. 5, the average GBS rate for these test conditions was calculated to be $\approx 1.3 \times 10^{-4}\ \mu m\ s^{-1}$. The average GBS rate was calculated by dividing the average cumulative GBS displacement measured by the creep time over which the GBS measurements were made. Recall

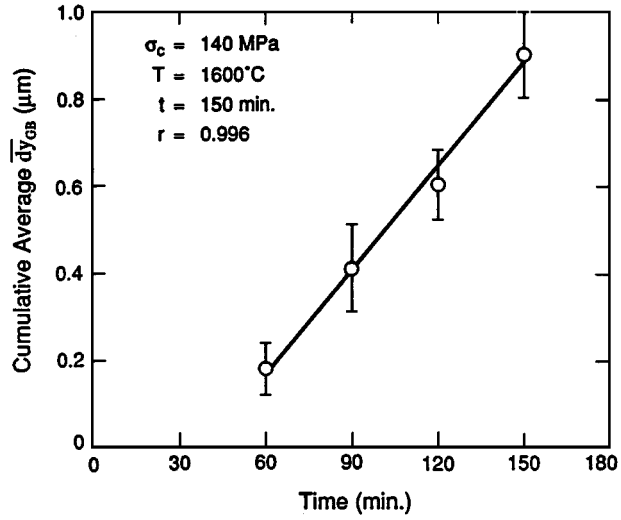

Figure 5 Cumulative average $\overline{dy}_{GB}$ (for 70 grain boundaries) versus time for the 140 MPa compressive creep specimen.

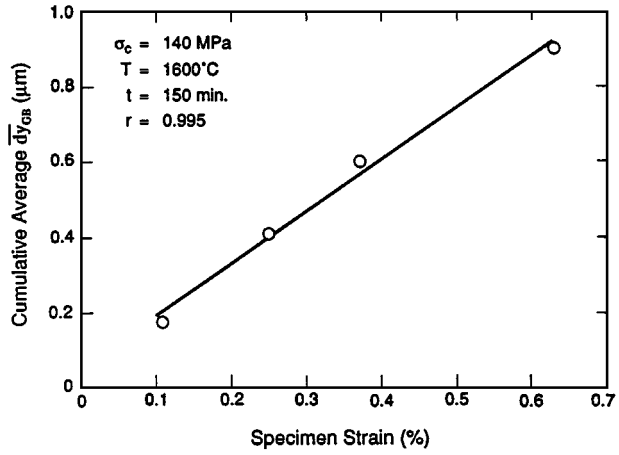

Figure 6 Cumulative average $\overline{dy}_{GB}$ versus specimen strain for the 140 MPa compressive creep specimen.

that the GBS data were not gathered during the 0–30 min time period because of a lack of surface features in the baseline microstructure. Therefore, the cumulative average $\overline{dy}_{GB}$ data may not be extrapolated to $\overline{dy}_{GB} = 0$ to determine the actual onset of GBS activity, as the cumulative average $\overline{dy}_{GB}$ values do not include any activity during the 0–30 min time period.

The cumulative average $\overline{dy}_{GB}$ also increases linearly with accumulated specimen strain, as shown in Fig. 6. This would be expected based on the relationship shown in Fig. 5 and the fact that the specimen was in the steady-state creep regime. The linear relationship between the cumulative average $\overline{dy}_{GB}$ and strain holds strong implications regarding both GBS behaviour and creep cavitation, as will be discussed.

As noted in Fig. 1, not all of the grain boundaries exhibited measurable sliding at each time interval. Therefore, in order to study the GBS activity, the percentage of grain boundaries exhibiting GBS is plotted versus creep-time interval in Fig. 7. For a given microstructural area, the fraction of boundaries measured that exhibited GBS either decreased or increased in successive time intervals, as observed in Fig. 7. For example, in area 3, 50% of the grain boundaries measured exhibited GBS

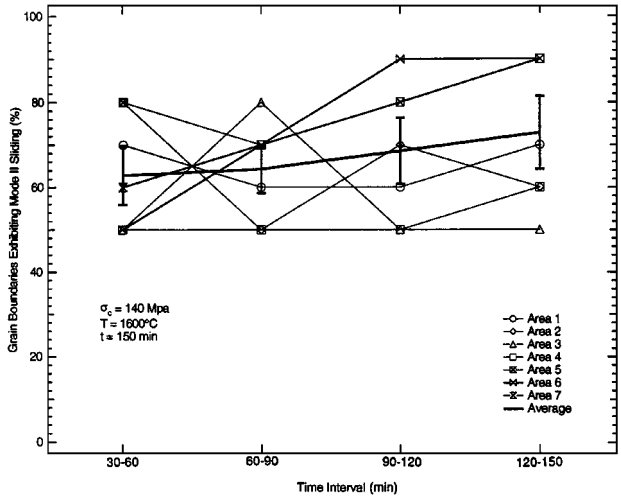

Figure 7 Percentage of grain boundaries exhibiting mode II sliding versus time interval for the seven areas of the microstructure measured. (The dark line shows the average over all of the areas with error bars of one standard deviation.)

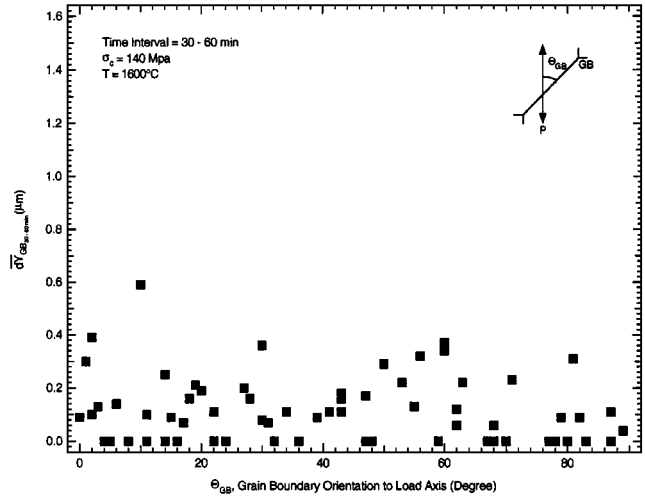

Figure 8 Magnitude of the mode II GBS displacement, $\overline{\mathrm{d}y}_{\mathrm{GB}}$, versus the respective grain boundary orientation to the load axis, θ_{GB}, for the 30–60 min time interval.

during the first time period. In the second time period, 80% of the boundaries slid, then 50% moved in the third and fourth periods. During any given creep time period in all seven areas, the GBS activity never decreased below 50%. The average percent of grain boundaries that exhibited mode II GBS over all seven areas (shown as the bold line) essentially remained constant within one standard deviation over creep time. However, it is interesting to note that the areas exhibiting a measurable increase in the average mode II sliding displacement over creep time, areas 5 and 7 (Fig. 2), also exhibited an increase in the fraction of boundaries that slid. Overall, $\approx 67\%$ of the grain boundaries measured in the 140 MPa specimen exhibited mode II GBS throughout the creep life of the specimen. Therefore, although the fraction of boundaries that slid in a given area was observed to vary somewhat over creep time, the overall average percentage of boundaries that slid remained relatively constant with creep time.

To determine if there is any preference of grain boundary orientation on the magnitude of mode II GBS displacement, $\overline{\mathrm{d}y}_{\mathrm{GB}}$, these values were plotted versus the grain boundary orientation to the load axis, θ_{GB}, for each creep time interval. This relationship for the 30–60 min measurements is shown in Fig. 8. When the mode II GBS displacements are plotted for each creep interval, there is no angular dependence observed. In fact, the magnitude of the sliding displacements is truly random with respect to θ_{GB}.

When the cumulative $\overline{\mathrm{d}y}_{\mathrm{GB}}$ for each grain boundary (summed over all four time intervals) is plotted versus θ_{GB}, an unclear pattern evolves, as shown in Fig. 9. Ninety-six percent of the data fall within the shaded region shown, suggesting the possibility that some correlation between $\overline{\mathrm{d}y}_{\mathrm{GB}}$ and θ_{GB} exists. In order to check this possible correlation, a null hypothesis was formulated: there is no correlation between $\overline{\mathrm{d}y}_{\mathrm{GB}}$ and θ_{GB}. The rank correlation statistical analysis, described by Kendall [49], was used to test the null hypothesis. Kendall's rank correlation [49] was also performed on a similar plot that was constructed using

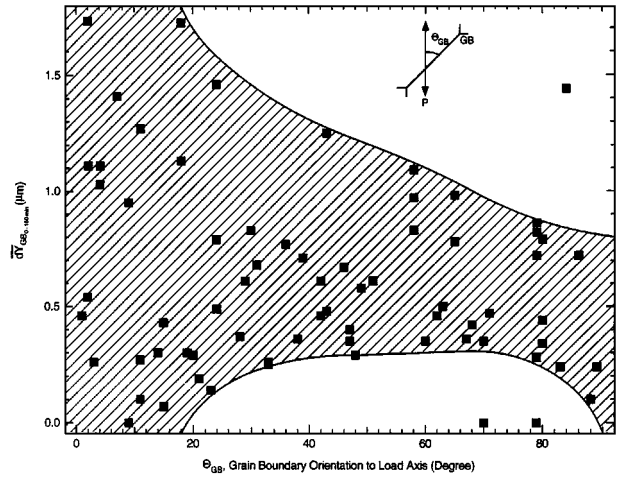

Figure 9 Cumulative mode II GBS displacement, $\overline{\mathrm{d}y}_{\mathrm{GB}}$, over all four time intervals versus the respective grain boundary orientation to the load axis, θ_{GB}.

randomly generated values of $\overline{\mathrm{d}y}_{\mathrm{GB}}$ and θ_{GB}. Briefly, correlation coefficients were calculated using both the random and experimental data. The resulting correlation coefficients for both the experimentally generated and randomly generated data were close to zero, thus providing sufficient reason to accept the null hypothesis: that no correlation exists between $\overline{\mathrm{d}y}_{\mathrm{GB}}$ and θ_{GB}, and that there is no dependence of the magnitude of mode II GBS displacements on the grain boundary orientation to the load axis.

3.3. 70 MPa test results

Although the 140 MPa tests were analysed in detail using a relatively large sampling of GBS measurements (70 grain boundaries), a small data sampling of GBS measurements (eight grain boundaries) was gathered on the 70 MPa specimen for comparative purposes.

In general, the GBS behaviour of the 70 MPa specimen was similar to that measured in the 140 MPa specimen. Specifically, GBS was observed to be stochastic and history independent. In addition, the average $\overline{\mathrm{d}y}_{\mathrm{GB}}$

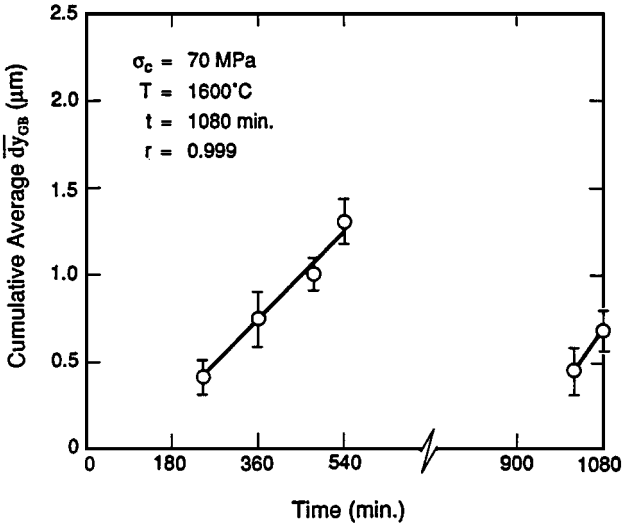

Figure 10 Cumulative average $\overline{\mathrm{d}y}_{\mathrm{GB}}$ versus time at a stress of 70 MPa.

measured during the 1080-min creep test remained constant within one standard deviation. Therefore, the cumulative average $\overline{\mathrm{d}y}_{\mathrm{GB}}$ increased linearly with time, as shown in Fig. 10. Thus, as with the 140 MPa test, cumulative GBS displacements increase linearly with creep time during steady-state creep at 70 MPa. Using these data, the GBS rate for the 70 MPa test was calculated to be $\approx 6 \times 10^{-5}\ \mu\mathrm{m\ s^{-1}}$. The same GBS rate was calculated for the two latter time periods used to measure GBS behaviour at a higher specimen strain (0.72%). Recall that the GBS rate measured in the randomly chosen areas on the 140 MPa specimen was $1.3 \times 10^{-4}\ \mu\mathrm{m\ s^{-1}}$, approximately two times that measured in the 70 MPa specimen. The cumulative average $\overline{\mathrm{d}y}_{\mathrm{GB}}$ also increases linearly with accumulated specimen strain for the 70 MPa specimen, as shown in Fig. 11.

4. Discussion

4.1. GBS behaviour

The results presented show that during compressive creep in Lucalox®, the GBS behaviour is stochastic and history independent. These findings are significant, as they are the first to document the GBS behaviour of individual grain boundaries in a polycrystalline ceramic during creep. Similar observations have been published in the metallurgy literature for bicrystals [50], and in the ceramic literature with one publication on NaCl and MgO bicrystals [30] that have led researchers [36] to assume that GBS is also stochastic in ceramic materials. In fact, in their modelling efforts, Chan and Page [36] assumed stochastic GBS induced periodic, short duration, stress spikes that acted as the driving force for continuous cavity nucleation during creep (in both metals and ceramics). Chan and Page [36] also assumed that the GBS behaviour "evolved without effects, i.e. the past sliding events have no influence on the future behaviour". This assumption was also observed to be true in this study, as GBS was shown to be history independent.

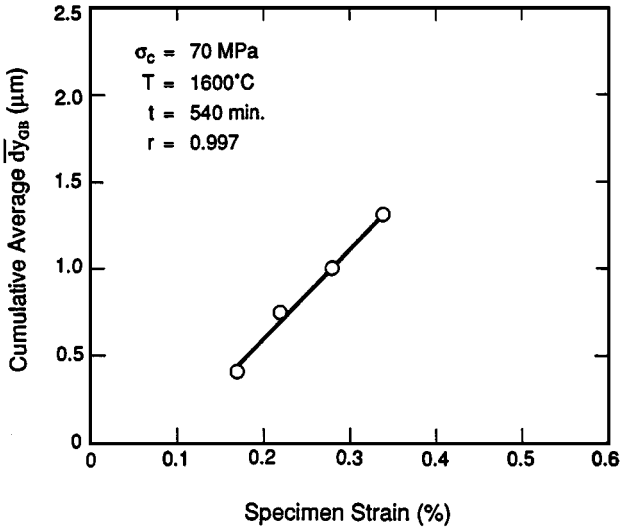

Figure 11 Cumulative average $\overline{\mathrm{d}y}_{\mathrm{GB}}$ versus specimen strain at a stress of 70 MPa.

The ramifications of the stochastic, history-independent GBS observed in this polycrystalline alumina system on the creep cavitation behaviour are also significant. Referring to the model developed by Chan and Page [36], they concluded that "stochastic GBS has been identified as the most likely driving force for continuous cavity nucleation in both metals and ceramics". These conclusions, based on a model, will be discussed in conjunction with experimental creep cavitation data in part II of this paper [1].

Previously, the lack of detailed GBS measurements in the literature forced the use of a term for the average cumulative GBS displacement. In Chan and Page's [36] model, $\langle x \rangle$ is used to symbolize the average sliding distance per sliding event and the average cumulative GBS displacement, $U(t)$, is

$$U(t) = \frac{a_o \langle x \rangle t^{1-m}}{(1-m)} \tag{4}$$

Earlier, the GBS measurements taken both at each time interval and over the entire specimen life were shown to fit a Weibull distribution. As such, Equation 4 can be made more accurate by replacing the $U(t)$ term with the actual distribution as follows: when $t = 150$ min and the measurements were initiated at $t = 30$ min

$$\begin{aligned} U(150) - U(30) &= f(\overline{\mathrm{d}y}_{\mathrm{GB}})_{\mathrm{cum}} \\ &= \frac{a_o \langle x \rangle [150^{1-m} - 30^{1-m}]}{(1-m)} \end{aligned} \tag{5}$$

where

$$f(\overline{\mathrm{d}y}_{\mathrm{GB}})_{\mathrm{cum}} = 2\left(\frac{\overline{\mathrm{d}y}_{\mathrm{GB}}}{0.72}\right)^{0.5} \exp\left[-\left(\frac{\overline{\mathrm{d}y}_{\mathrm{GB}}}{0.72}\right)^{1.5}\right] \tag{6}$$

When treated rigorously, $\langle x \rangle$ is the average sliding distance per individual sliding event. This quantity is difficult to measure with the techniques currently available.

During steady-state creep, the average $\overline{\mathrm{d}y}_{\mathrm{GB}}$ remained constant in the microstructural areas used for the GBS measurements. As a result, the cumulative

average $\overline{dy}_{GB}$ was shown to increase linearly with time and specimen strain. Therefore, GBS was shown to be a steady-state process, meaning $m = 0$ in Equation 4 . Similar GBS behaviour has been observed on a variety of polycrystalline metals [51]. In fact, with the longer primary and tertiary creep regimes found in most metals (compared to ceramics), the mean GBS displacement versus time curve has been shown to closely resemble the actual specimen displacement versus time creep curves [52] throughout each creep regime.

4.2. Effect of grain boundary orientation on GBS

It was shown that there is no preference of grain boundary orientation (to the compressive load axis) on the magnitude of the respective mode II GBS displacement, $\overline{dy}_{GB}$. In fact, $\overline{dy}_{GB}$ was found be random versus θ_{GB} at each time interval and for the cumulative (30–150 min) data.

Generally, two schools of thought exist on this subject, but are only alluded to in the literature addressing ceramic materials undergoing creep. One suggests that no relationship exists between relative grain motion and orientation to the load axis due to compatibility and constraint requirements [5]. The second point of view is that a grain boundary with a 90° orientation to the load axis should experience little grain boundary sliding because of the minimum resolved shear stress, whereas a boundary with a 45° orientation should exhibit maximum displacement because of the maximum resolved shear stress [11, 53]. Although many researchers attempting to model GBS and related phenomenon use the simple geometric approach to resolve local stresses, it is generally accepted, and further supported by the results of this study, that compatibility and constraint requirements rule the overall GBS process during compressive creep [11, 53]. It is obvious from the analysis of Figs 8 and 9 that no correlation exists between the magnitude of displacement at a given grain boundary and its orientation to the load axis. In fact, contrary to the second school of thought, the largest $\overline{dy}_{GB}$ values were observed on boundaries nearly perpendicular and parallel to the load axis, and the remaining measured displacements (on boundaries oriented between 0 and 90°) varied substantially. These results suggest that GBS and other relative grain movements are dictated by grain compatibility requirements, and may be random with respect to orientation. Also, no orientation preference was observed for either sliding or non-sliding.

Blanchard and Page [18] previously published GBS data showing relative grain movements in one microstructural area during one 30-min creep interval. No apparent relationship was observed between the magnitude and direction of the relative grain movements and the orientation of the load axis, and no obvious trends in relative grain motion in two dimensions were observed. It is interesting to note that apparent contradicting movements and negative sliding are depicted in the micrograph they show. Negative sliding may be a result of grain rotation or a compatibility requirement caused by the motion of the adjacent ridged, elastic grains.

TABLE II Compressive creep and GBS characteristics

Applied stress (MPa)	Total strain (%)	Strain rate (s^{-1})	GBS rate ($\mu m\ s^{-1}$)
140	0.63	7×10^{-7}	1.3×10^{-4}
70	0.72	1×10^{-7}	6.0×10^{-5}

4.3. Effect of applied stress on GBS

GBS measurements were made on compressive creep specimens tested at only two stress levels, 70 and 140 MPa. Without GBS data obtained at a third stress level, the true stress dependence of GBS behaviour could not be quantified. But, by comparing the data obtained at 70 and 140 MPa, shown in Table II, some general observations may be made.

As previously stated, GBS behaviour both at a 70 MPa and 140 MPa load was observed to be stochastic and history dependent. In addition, the average $\overline{dy}_{GB}$ measured remained essentially constant with creep time at both loads. Therefore, the cumulative average $\overline{dy}_{GB}$ was observed to increase linearly with time and strain during steady-state creep at both loads. Comparing the GBS rates measured at each load level reveals that at 140 MPa, the GBS rate was twice that measured at 70 MPa.

Only one reference to the stress dependence of GBS for a ceramic material (MgO) is available in the literature [32]. In this report, Langdon [32] simply states that "grain-boundary sliding increases in importance with decreasing stress". This statement was substantiated with measurements of ϵ_{gb}/ϵ_t (the contribution of GBS to the total creep strain) of 20% at a stress of 34 MPa, 8% at 69 MPa, and 7% at 103 MPa. Unfortunately, Langdon did not report a GBS rate, thereby preventing the formulation of the true stress dependence on GBS. Langdon's results do, however, illustrate the importance of the GBS phenomenon in ceramics at relatively low stress levels, conditions often employed for long-service structural components.

In the metallurgy literature, similar GBS measurements on a Mg alloy, Magnox Al80 [52], and pure Al [54], also showed that the contribution of GBS to the total creep strain (ϵ_{gb}/ϵ_t) increased as the stress decreased. In addition, for very low stresses (less than 0.14 MPa), Harper *et al.* [54] noted that ϵ_{gb}/ϵ_t decreases with decreasing stress because of "the distinct differences in crystallographic mechanisms for creep in the low stress ranges".

Only two studies providing the actual stress dependence of the GBS rate have been reported thus far [55, 56]. In both cases, the data were measured on a Pb bicrystal system. Although not highly representative of a polycrystalline ceramic, the GBS behaviour of the Pb bicrystal system was similar to the Lucalox® system reported here, and is thus worth discussing. By plotting their data, Gifkins and Snowden [55] showed that the relationship between the rate of sliding and stress

and the relationship between the creep rate and stress followed the same behavior. Specifically, the stress dependence of the steady-state creep rate is described by a power law as follows [55]

$$\dot{\epsilon} = A\sigma^n \tag{7}$$

where A is a constant, σ the applied stress, and n the stress exponent. The stress dependence of the GBS rate was therefore described by Strutt *et al.* [56] as follows

$$\dot{P} = C\sigma^\beta \tag{8}$$

where $\dot{P}$ is the GBS rate, C is a constant and β is the stress exponent for GBS. At stresses of 0.69–2.1 MPa, Pb bicrystals exhibit an $n = 1$; therefore, the GBS rate is linear with stress. Above 2.1 MPa, $n \cong 5$, and the GBS rate increases approximately with the stress cubed. Without further GBS measurements at a third stress level, it can only be hypothesized that the GBS behavior of the Lucalox® follows the relationship in Equation 8.

5. Conclusions

The data presented in this paper reveal a number of important characteristics about GBS behavior in a structural ceramic undergoing creep. The sliding measurements performed on individual grains during the compressive creep process confirm that GBS is, in fact, stochastic, or random over time, and history independent. In addition, at any point in time during creep, almost 70% of the grain boundaries measured exhibited some magnitude of GBS. Grain boundary sliding displacements measured at given time intervals were shown to best fit a Weibull distribution defined by α and β values of 1.45 and 0.25, respectively. No correlation was found to exist between the magnitude of GBS displacements and the grain boundary orientation to the load axis. At stress levels of both 140 and 70 MPa, the average magnitude of GBS displacement ($\overline{dy}_{GB}$) was shown to remain constant over creep time. Therefore, it was also shown that during steady-state compressive creep, the cumulative GBS displacements increase linearly with creep time and strain. This provides direct evidence that GBS provides a continuous and accumulative damage mechanism in ceramics undergoing creep, thus meeting a significant criterion as a driving force for creep cavitation. The rate of GBS in the 70 MPa test was half of that measured in the 140 MPa test. More work is needed to define the stress dependence of GBS. In part II of this paper [1], the GBS measurements reported will be related to corresponding creep cavitation measurements to provide more evidence to suggest that GBS is the driving force for creep cavitation.

Acknowledgements

The authors are grateful for the support of this work by the Southwest Research Institute Internal Research Program. The technical contributions of Messrs J. Sievert and R. Railsback are also greatly appreciated.

References

1. C. R. BLANCHARD and R. A. PAGE, *J. Mater. Sci.* **33** (1998) 5049.
2. A. G. EVANS, in "Recent Advances in Creep and Fracture of Engineering Materials and Structures," edited by B. Wilshire and D. R. J. Owen (Pineridge Press, Swansea, UK, 1982) p. 53.
3. A. H. CHOKSHI and T. G. LANGDON, *Mater. Sci. Tech.* **7** (1991) 577.
4. J. R. PORTER, W. BLUMENTHAL and A. G. EVANS, *Acta Metall.* **29** (1981) 1899.
5. K. JAKUS, S. M. WIEDERHORN and B. J. HOCKEY, *J. Amer. Ceram. Soc.* **69** (1986) 725.
6. R. A. PAGE, J. LANKFORD, K. S. CHAN, K. HARDMAN-RHYNE and S. SPOONER, *ibid.* **70** (1987) 137.
7. R. RAJ, in "Advances in Fracture Research," Vol. 4, edited by K. Salama, K. Ravichandar, D. M. R. Toplin, and P. Rama Rao (Pergamon Press, New York, 1989) p. 2769.
8. K. S. CHAN and R. A. PAGE, *J. Amer. Ceram. Soc.* **76** (1993) 803.
9. J. INTRATER and E. S. MACHLIN, *Acta Metall.* **7** (1959) 140.
10. R. RAJ, *ibid. Acta* **26** (1978) 995.
11. K. S. CHAN, R. A. PAGE and J. LANKFORD, *ibid. Acta Metall.* **34** (1986) 2361.
12. R. A. PAGE and K. S. CHAN, *Metall. Trans. A* **18A** (1987) 1843.
13. C. R. BLANCHARD and K. S. CHAN, *J. Amer. Ceram. Soc.* **76** (1993) 1651.
14. R. G. FLECK, D. M. R. TAPLIN and C. J. BEEVERS, *Acta Metall.* **23** (1975) 415.
15. A. H. CHOKSHI, *J. Mater. Sci.* **25** (1990) 3221.
16. F. WAKAI and H. KATO, *Adv. Ceram. Mater.* **3** (1988) 71.
17. C. R. BLANCHARD and R. A. PAGE, *J. Mater. Sci.* **26** (1991) 3165.
18. *Idem., J. Amer. Ceram. Soc.* **75** (1992) 1612.
19. C. R. BLANCHARD, PhD Dissertation, The University of Texas at Austin, 1994.
20. S. M. COPLEY and J. A. PASK, *J. Amer. Ceram. Soc.* **48** (1965) 636.
21. J. H. HENSLAR and G. V. CULLEN, *ibid.* **50** (1967) 584.
22. T. SUGITA and J. A. PASK, *ibid.* **53** (1970) 609.
23. H. C. HEARD and C. B. RALEIGH, *Geol. Soc. Amer. Bull.* **83** (1972) 935.
24. M. TOKAR, *J. Amer. Ceram. Soc.* **56** (1973) 173.
25. T. G. LANGDON, *ibid.* **58** (1975) 92.
26. W. R. CANNON and O. D. SHERBY, *ibid.* **60** (1977) 44.
27. F. WAKAI and H. KATO, *Adv. Ceram. Mater.* **3** (1988) 71.
28. R. D. NIXON and R. F. DAVIS, *J. Amer. Ceram. Soc.* **75** (1992) 1786.
29. *Idem., ibid.* **75** (1992) 1786.
30. M. A. ADAMS and G. T. MURRAY, *J. Appl. Phys.* **33** (1962) 2126.
31. P. F. BECHER and H. PALMOUR III, *J. Amer. Ceram. Soc.* **53** (1970) 119.
32. T. G. LANGDON, *ibid.* **58** (1975) 92.
33. R. RAJ and M. F. ASHBY, *Acta Metall.* **23** (1975) 653.
34. A. S. ARGON, I. W. CHEN and C. W. LAU, in "Creep–fatigue–environment interaction," edited by R. M. Pelloux and N. S. Stoloff (Metallurgical Society of AIME, New York, 1980) p. 46.
35. A. S. ARGON, *Scripta Metall.* **17** (1983) 5.
36. K. S. CHAN and R. A. PAGE, *J. Mater. Sci.* **25** (1990) 4622.
37. *Idem., J. Mater. Sci.* **27** (1992) 1651.
38. H. M. KARRARA (ed.), "Handbook of non-topographic photogrammetry" (American Society for Photogrammetry, Falls Church, VA, 1979).
39. D. L. DAVIDSON, *Acta Metall.* **36** (1988) 2275.
40. K. S. CHAN and D. L. DAVIDSON, *Engng. Fract. Mech.* **33** (1989) 451.
41. D. L. DAVIDSON, *ibid.* **25** (1986) 123.
42. D. L. DAVIDSON and J. LANKFORD, *Mater. Sci. Engng.* **60** (1983) 225.
43. H. L. MARCUS and M. E. FINE, *J. Amer. Ceram. Soc.* **55** (1972) 568.
44. W. C. JOHNSON, *Met. Trans. A* **8A** (1977) 1413.

45. E. A. FRANKE, D. J. WENZEL and D. L. DAVIDSON, *Rev. Sci. Instrum.* **62** (1991) 1270.
46. P. H. WIRSCHING and J. R. CARLSON, *J. Engng. Mech. Div. Amer. Soc. Civ. Eng.* **103** (1977) 125.
47. J. M. FINKELSTEIN and R. E. SCHAFER, *Biometrika* **58** (1971) 641.
48. W. WEIBULL, *J. Appl. Mech.* **18** (1951) 293.
49. M. G. KENDALL, *Biometrika* **30** (1938) 81.
50. J. INTRATER and E. S. MACHLIN, *J. Inst. Metals.* **88** (1959-1960) 305.
51. H. GLEITER and B. CHALMERS, in "Progress in materials science incorporating Progress in metal physics," Vol. 1b, edited by B. Chalmers, J. W. Christian and T. B. Massalski (Pergamon Press, Oxford, 1972) p. 179.
52. R. L. BELL and T. G. LANGDON, *J. Mater. Sci.* **2** (1967) 313.
53. R. RAJ and M. F. ASHBY, *Met. Trans.* **2** (1971) 1113.
54. J. G. HARPER, L. A. SHEPARD and J. E. DORN, *Acta Metall.* **6** (1958) 509.
55. R. C. GIFKINS and K. U. SNOWDEN, *Trans. Metall. Soc. AIME* **239** (1967) 910.
56. P. R. STRUTT, A. M. LEWIS and R. C. GIFKINS, *J. Inst. Metals* **93** (1964-1965) 71.

Received 7 February 1997
and accepted 1 June 1998